

Viscous and Inviscid Reconnection of Vortex Rings on Logarithmic Lattices

Abhishek Harikrishnan, Adrien Lopez, Bérengère Dubrulle

Université Paris-Saclay, CEA, CNRS, SPEC, 91191, Gif-sur-Yvette, France

Abstract

To address the possible occurrence of a Finite-Time Singularity (FTS) during the oblique reconnection of two vortex rings, Moffatt-Kimura (MK) (*J. Fluid Mech.*, 2019a; *J. Fluid Mech.*, 2019b) developed a simplified model based on the Biot-Savart law and claimed that the vorticity amplification ω_{\max}/ω_0 becomes very large for vortex Reynolds number $Re_\Gamma \geq 4000$. However, with Direct Numerical Simulation (DNS), Yao and Hussain (*J. Fluid Mech.*, 2020) were able to show that the vorticity amplification is in fact much smaller and increases slowly with Re_Γ . The suppression of vorticity was linked to two key factors - deformation of the vortex core during approach and formation of hairpin-like bridge structures. In this work, a recently developed numerical technique called *log-lattice* (Campolina and Mailybaev, *Nonlinearity*, 2021), where interacting Fourier modes are logarithmically sampled, is applied to the same oblique vortex ring interaction problem. It is shown that this technique is not only capable of capturing the two key physical processes overlooked by the MK model but also other quantitative and qualitative attributes generally seen with DNS, at a fraction of the computational cost. Furthermore, the sparsity of the Fourier modes allows us to probe very large $Re_\Gamma = 10^8$ until which the peak of the maximum norm of vorticity, while increasing with Re_Γ , remains finite, and a blowup is observed only for the inviscid case.

1 Introduction

Vortex reconnection is described by Yao and Hussain [2020a] as a “fundamental topology-transforming dynamical event”. Studying its mechanism is important for predicting the behavior of trailing vortices of an aircraft, understanding the turbulence cascade and more importantly, the occurrence of finite-time singularities (FTS) in Euler or Navier-Stokes equations [Yao and Hussain, 2022]. The starting configuration ranges from simple vortex rings and vortex tubes to complex knotted and linked vortices such as the Hopf link and the trefoil knot. Numerical simulations are usually carried out with either direct numerical simulation (DNS) or simplified models.

With a Biot-Savart (B-S) model, Kimura and Moffatt [2017] and references therein, found that anti-parallel vortex filaments stretch out as they approach closely forming a tent-like (or pyramid-like) structure before reconnection regardless of the initial configuration, thereby suggesting a universal route. To desingularize the B-S integral, a ‘cut-off’ parameter is added to the denominator. This implies that the integral will produce spurious results for length scales smaller than the cut-off, such as at the time of reconnection. Moffatt and Kimura [2019a] argued that the evolution at reconnection time depends only on the curvature, the core radius and the separation distance. They used the B-S law to obtain analytical expressions for the rate of change of these variables, resulting in a non-linear dynamical system, hereafter referred as the MK model. With this and subsequent work [Moffatt and Kimura, 2019b], they suggested the possible occurrence of ‘physical’ singularity for both inviscid (Euler) flow and viscous flows when the vortex Reynolds number $Re_\Gamma = \Gamma/\nu \geq 4000$. Here, Γ is the circulation strength and ν is the kinematic viscosity. In particular, they note that the vorticity amplification, i.e., the ratio of maximum vorticity at some time t_c to the initial vorticity ω_{\max}/ω_0 , takes very large values with increase in Re_Γ . This is important as it was shown with the theorem of Beale et al. [1984] that if a FTS occurs at a critical time t_c , then the maximum norm of vorticity becomes unbounded, i.e., $\int_0^{t_c} \|\boldsymbol{\omega}(\mathbf{x}, t)\|_\infty = \infty$. Employing a similar setup with Re_Γ up to 4000, Yao and Hussain [2020b], hereafter YH, used DNS to show that the vorticity amplification is, in fact, much smaller than that reported by Moffatt and Kimura [2019b]. In particular, YH attributed the suppression of vortex growth to flattening of the vortex cores as they approach closely and the braking effect of the bridges, both of which were ignored in the MK model.

Early work with DNS at low Re_Γ , for instance Kida et al. [1991], were instrumental in establishing a clear understanding of the physical mechanism of reconnection. The process is usually divided into three phases. In the first phase called *inviscid advection*, the vortex rings approach each other due to self-and mutual induction and they undergo strong vortex stretching. The cores also flatten resulting in a dipole structure. Next, during the *bridging* phase, the antiparallel vortex lines annihilate each other resulting in the formation of bridge-or hairpin-like structures in a direction orthogonal to the interaction. While the bridge structures rapidly recede away, they still remain connected by remnant threads from incomplete reconnection, resulting in the *threading* phase. High $Re_\Gamma \leq 40,000$ simulations with vortex tubes [Yao and Hussain, 2020a, 2022] have revealed more intricate details with increasing Re_Γ such as the formation of the $k^{-5/3}$ spectrum as a result of successive reconnections and the core flattening becoming more pronounced. Since DNS may become prohibitively expensive for larger Re_Γ , it is useful to have a simplified model capable of preserving the important physical processes elucidated above while being computationally cheaper.

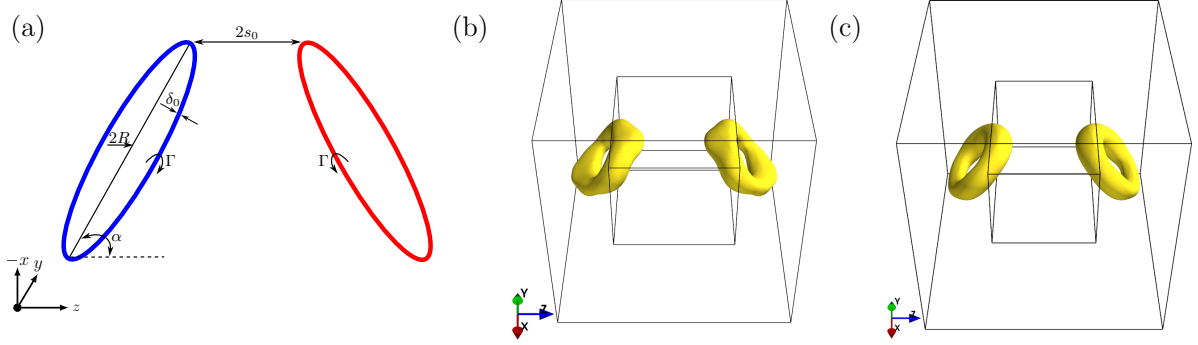


Figure 1: (a) Schematic of the initial configuration. Figure adapted from YH. (b) Visualization of vortex rings from log-lattices for the Kida-type ring with $\delta_0/R = 0.2$ with the spacing factor $\lambda = \phi$, (c) $\lambda \approx 1.194$. Q-criterion isosurfaces on a grid of size 128^3 are plotted at $Q > 0.35 Q_{\max}$ and $Q > 0.3 Q_{\max}$ respectively.

In this paper, we use a projection of Navier-Stokes equations on a set of logarithmically spaced discrete Fourier modes to achieve very large Reynolds number, at moderate numerical cost. Such projection was invented by Campolina and Mailybaev [2021] and termed logarithmic-lattice (or log-lattice, in short). Although it may superficially look like a mere 3D generalization of well-known shell models of turbulence (see review by Biferale [2003]), the projection on log-lattice is a mathematically well defined procedure, allowing to preserve the main symmetries and conservation laws of the original equations, without the need of adjustable parameters. The interest of this technique for the problem of FTS has already been demonstrated by Campolina and Mailybaev [2018] who showed that Euler equation on log-lattice develops a blow-up at finite time. The blow-up is characterized by a chaotic attractor, that spans a wide range of scales, out-of-reach of present DNS (see figure 2 of Campolina and Mailybaev [2018]). This unique combination of using the equations of motion in their original form and the ability to span a wide range of scales with few modes makes log-lattice an attractive tool for studying vortex reconnections and its links to FTS.

In this work, initial conditions similar to Moffatt and Kimura [2019a] and Kida et al. [1991] are used to study some quantitative and qualitative aspects of oblique reconnection of vortex rings for $Re_\Gamma \rightarrow \infty$ with log-lattices. The qualitative studies require reconstruction of physical space from lattice variables which is currently an open question. Previous studies with shell models [Bohr et al., 1998, Gürçan, 2017] have suggested employing the standard discrete Fourier transform to reconstruct the velocity field in physical space. This method described in subsection 2.2 is useful to verify the initial conditions (cf. subsection 2.3) that need to be described directly in Fourier space. Along with the qualitative studies, temporal behavior of global quantities such as enstrophy \mathcal{E} and maximum norm of vorticity $\|\omega\|_\infty$ with increasing Re_Γ are discussed in section 3.

2 Numerical framework and initial conditions

2.1 Log-lattice framework

Only a brief description of the log-lattice framework is given here. Additional details can be found in Campolina and Mailybaev [2021]. Starting with the Fourier transform of the

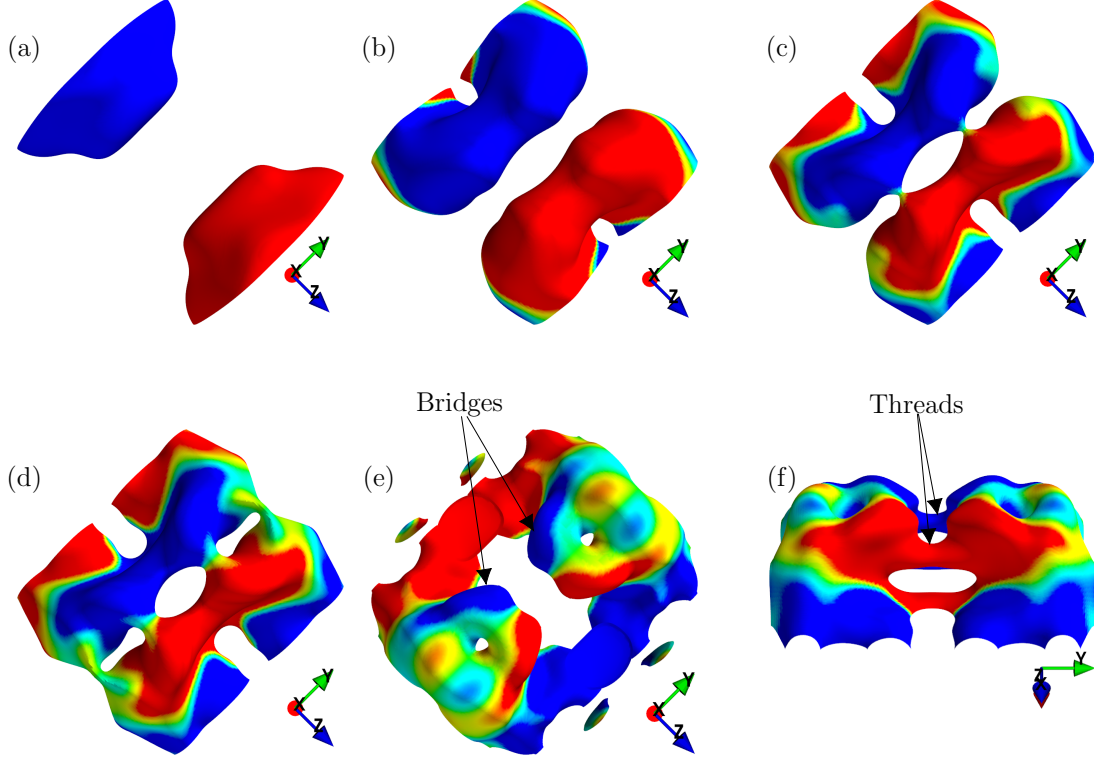


Figure 2: Q-criterion isosurfaces shaded with contours of axial vorticity at $t = \{0.005, 0.118, 0.162, 0.175, 0.222, 0.201\}$ thresholded at $Q > 0.1Q_{\max}$. Only a small portion of the domain is visualized as shown in figure 1(b).

incompressible Navier-Stokes equation,

$$\partial_t u_i + \mathbf{i} k_j u_i * u_j = -\mathbf{i} k_i p - \nu k^2 u_i + f_i, \quad (1)$$

$$\mathbf{i} k_j u_j = 0, \quad (2)$$

$$u_i * u_j(k) = \sum_{\substack{q, r \in \Lambda^3 \\ q+r=k}} u_i(q) u_j(r) \quad (3)$$

where $\mathbf{i} = \sqrt{-1}$, k_i is the i th component of the d -dimensional wave vector $\mathbf{k} = (k_1, \dots, k_d)$, p is the complex pressure field, f_i denotes the forcing and ν is the kinematic viscosity. In this work, $f_i = 0$ for all simulations. When $\nu = 0$, the flow is inviscid and the system reduces to the incompressible Euler equations. Here, (3) describes the main convolution operation which couples Fourier modes in triadic interactions such that $k = q + r$ and q, r, k are any three nodes on a *logarithmic lattice* Λ . The logarithmic lattice is the set,

$$\Lambda = \{\pm \lambda^n\}_{n \in \mathbb{Z}} \quad (4)$$

where $\lambda > 1$ is the spacing factor. As shown in Campolina and Mailybaev [2021], nontrivial triad interactions exist only when the equation $\lambda^n = \lambda^q + \lambda^r$ has integer solutions for any $(n, q, r) \in \mathbb{Z}^3$. The following three families of solutions are known to exist, each with z interactions in d -dimensions:

(i) $\lambda = 2$ with $z = 3^d$

(ii) $\lambda = \sigma \approx 1.325$ is the plastic number with $z = 12^d$

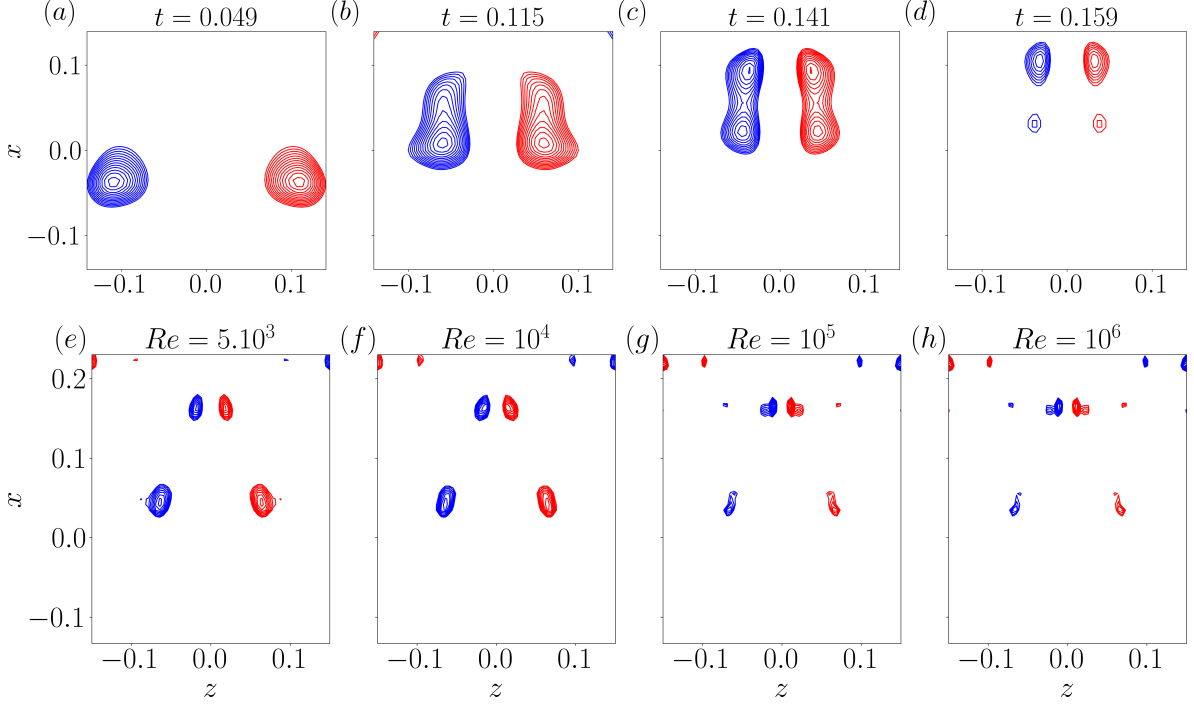


Figure 3: (a-d) Temporal evolution of the vortex core shape is shown with contours of axial vorticity with level sets $\omega_y = [0.75 - 0.99]\omega_{y,\max}$ in the symmetric (x, z) plane for the Kida-type ring at $Re_\Gamma = 10^4$. (e-h) Contours of axial vorticity at $t = 0.115$ and level sets $\omega_y = [0.85 - 0.99]\omega_{y,\max}$ is shown in the symmetric (x, z) plane for the MK-type ring for increasing Re_Γ .

- (iii) Any λ that satisfies $1 = \lambda^b - \lambda^a$ where (a, b) are mutual prime integers and $(a, b) \neq (1, 3), (4, 5)$. In this case, $z = 6^d$. For $(a, b) = (1, 2)$, the spacing factor $\lambda = \phi \approx 1.618$ is the golden mean.

While decreasing the spacing factor λ can increase the node density and the number of interactions per node which is desirable for simulating turbulent flows, this increases the computational cost. In this sense, simulations with $\lambda = 2$ are computationally cheaper but as pointed out in Barral and Dubrulle [2023], it should be avoided for divergence-free flows because of the lack of backscatter.

In this work, $\lambda = \phi$ is chosen for all simulations. The minimum wave vector k_{\min} is set to 2π to match a simulation on a box of size $L = 1$. The initial grid size is set as $(2N)^3 = 40^3$ for simulations without the zero component modes \mathbf{k}_0 . The code is adaptive and the grid size is updated based on the fraction of energy contained in the outermost shells. The computational cost is reduced further by taking advantage of the grid symmetry along the initial axis $f(-k) = \overline{f(k)}$ where $\overline{(\cdot)}$ denotes complex conjugation. This means that the actual simulation is performed for $N \times 2N \times 2N$ nodes instead of $(2N)^3$ nodes for each velocity component.

2.2 Flow visualization with log-lattice

To enable qualitative studies, 3D velocity fields need to be reconstructed in physical space from the lattice variables. As suggested in Bohr et al. [1998], Gürçan [2017], a

simple algorithm would involve the discrete Fourier transform (DFT),

$$\mathbf{u}(\mathbf{x}) = \sum_{\mathbf{k} \in \Lambda} \hat{\mathbf{u}}(\mathbf{k}) \cdot e^{i\mathbf{k} \cdot \mathbf{x}} \quad (5)$$

where $\hat{\mathbf{u}}(\mathbf{k})$ is the velocity vector in Fourier space, \mathbf{k} is the non-uniformly spaced wave vector, \mathbf{x} are evenly-spaced sample points. If Λ is an evenly-spaced lattice, then (5) reduces to the regular DFT. While the complexity of the regular one-dimensional DFT is $\mathcal{O}(N^2)$, the complexity for log-lattices is $\mathcal{O}(N \log_\lambda N)$, similar to a Fast-Fourier transform, which reduces computation time. However, for large number of sample points, this is still computationally expensive and therefore, the python DFT code was GPU-parallelized with the CuPy library.

2.3 Initial conditions and simulation details

Two sets of initial conditions are chosen to study the oblique interaction of two vortex rings as shown in figure 1(a). The first set is similar to MK with initially circular vortex rings with radii R , thickness δ_0 and inclination angle $\alpha = 45^\circ$. They have equal and opposite circulation Γ and are separated at from their centerlines by a distance $2s_0 = 0.4$. The core size is $\delta_0/R = 0.01$. The only difference with the second set is the core size which is $\delta_0/R = 0.2$ which is similar to that studied by Kida et al. [1991]. The larger core size enables better visualization of the various reconnection processes.

Due to the spectral nature of log-lattices, the initial conditions need to be described in Fourier space as well. This immediately leads to the question of how to represent a vortex ring structure in Fourier space. An early idea exploited the fact that the Fourier transform of a 3D Gaussian function is another 3D Gaussian, and a rudimentary ring can be constructed by imposing the divergence-free condition. However, this type of ring has essentially one length scale to control its thickness but the radius of the ring cannot be controlled. The current idea makes use of the Dirac delta function to represent a 2D circle in 3D space. For a vortex ring of radius R , the vorticity is given by,

$$\boldsymbol{\omega}(\mathbf{x}) = \Gamma \int \delta^{(3)}(\mathbf{x} - \mathbf{R}(\phi)) d\mathbf{R}(\phi) d\phi \quad (6)$$

where $\mathbf{R}(\phi) = (R \cos \phi, R \sin \phi, 0)$ and the unit tangent vector $d\mathbf{R}(\phi) = (-\sin \phi, \cos \phi, 0)$. Taking the Fourier transform of (6),

$$\hat{\boldsymbol{\omega}}(\mathbf{k}) = \Gamma \int e^{-i\mathbf{k} \cdot \mathbf{R}(\phi)} d\mathbf{R}(\phi) d\phi \quad (7)$$

Using polar coordinates with $x = R \cos \phi$, $y = R \sin \phi$ and correspondingly $k_x = k_\perp \cos \alpha$, $k_y = k_\perp \sin \alpha$ such that $R = \sqrt{x^2 + y^2}$ and $k_\perp = \sqrt{k_x^2 + k_y^2}$, the dot product $\mathbf{k} \cdot \mathbf{R}(\phi)$ reduces to $Rk_\perp \cos(\phi - \alpha)$ and (7) can be written as,

$$\hat{\boldsymbol{\omega}}(\mathbf{k}) = \Gamma \int e^{-iRk_\perp \cos(\phi - \alpha)} [-\sin \phi, \cos \phi, 0] d\phi \quad (8)$$

Let $\theta = \phi - \alpha$ such that $d\theta = d\phi$ and after some trigonometric manipulation, we note that the result $\int e^{iRk_\perp \cos \theta} \cos \theta d\theta$ can be conveniently expressed as a Bessel function $-iJ_1(k_\perp R)$. Further, assuming $\Gamma = 1$ and convolving with a 3D Gaussian of width δ_0

to represent the thickness of the vortex ring, the following closed-form expressions are obtained,

$$\hat{\omega}(k_x) = -iJ_1(k_\perp R) \frac{k_y}{k_\perp} e^{\frac{-(\|\mathbf{k}\|\delta_0)^2}{2}} \quad (9)$$

$$\hat{\omega}(k_y) = iJ_1(k_\perp R) \frac{k_x}{k_\perp} e^{\frac{-(\|\mathbf{k}\|\delta_0)^2}{2}} \quad (10)$$

This describes a single vortex ring in Fourier space having radius R and thickness δ_0 oriented along the z -direction. Straightforward extensions of the formula allow for translation and rotation of the ring. For instance, to translate the ring in the $-z$ direction by a distance s_0 , one can convolve (9 - 10) with $e^{-ik_z s_0}$. Multiple rings can be added by superposition. Finally, the initial velocity field can be obtained by applying the Biot-Savart law,

$$\hat{\mathbf{u}}(\mathbf{k}) = \frac{i\mathbf{k} \times \hat{\boldsymbol{\omega}}(\mathbf{k})}{\|\mathbf{k}\|^2} \quad \text{for } \mathbf{k} \neq 0 \quad (11)$$

To study the qualitative aspects of reconnection, one needs to define a vortex. In this work, the second invariant of the velocity gradient tensor $\nabla \mathbf{u}$, i.e., the Q-criterion [Hunt et al., 1988] is chosen, which identifies vortices as regions where rotation dominates over the strain,

$$Q = \frac{1}{2}(\|\boldsymbol{\Omega}\|^2 - \|\mathbf{S}\|^2) > 0 \quad (12)$$

where $\boldsymbol{\Omega} = \frac{1}{2}[\nabla \mathbf{u} - (\nabla \mathbf{u})^T]$ is the spin tensor and $\mathbf{S} = \frac{1}{2}[\nabla \mathbf{u} + (\nabla \mathbf{u})^T]$ is the strain-rate tensor. This can be seen as an immediate improvement over vorticity magnitude $\|\boldsymbol{\omega}\| = \|\nabla \times \mathbf{u}\|$, which is known to misidentify shearing motions as vortices as both regions possess non-zero vorticity [Lugt, 1979]. While numerous works in the vortex reconnection literature appear to favor the λ_2 criterion, which identifies regions as vortices when the middle eigenvalue λ_2 of the symmetric tensor $(\mathbf{S}^2 + \boldsymbol{\Omega}^2)$ possess negative values $\lambda_2 < 0$, Chakraborty et al. [2005] showed that it is possible to obtain equivalent thresholds among popular methods such as the Q, λ_2 and Δ criteria so that a particular choice among these criteria should not affect the qualitative results presented here.

The initial conditions for the Kida-type ring with $\delta_0/R = 0.2$, after applying the inverse DFT is visualized with the Q-criterion 1(b). Applying a threshold $Q > 0.35Q_{\max}$ reveals the vortex rings. One can take advantage of the fact that large scale modes are grouped closer on a logarithmic grid to ensure better physical space representation. This means using rings with large radii (for instance $R = 0.1L$ where L is the integral scale) and large thickness lead to a better result. Further improvements can be made at the expense of increased computational cost, for instance, including the modes containing zero components \mathbf{k}_0 and reducing the grid spacing factor λ . All visualizations in this manuscript are shown with simulations performed with the \mathbf{k}_0 modes. The effect of reducing λ can be seen from figure 1(c) where the rings appear more circular than 1(b). Due to the irregular spacing of the Fourier modes, using the inverse DFT also introduces artefacts/images with lower amplitude which are generally not visible at larger thresholds but become more apparent as the simulation progresses and turbulence decays. All visualizations and plots produced with real space data were made early times where the impact of these artefacts were negligible. To track the behavior of global quantities such as enstrophy and maximum norm of vorticity over long time, they were calculated directly in Fourier space which is unaffected by the artefacts.

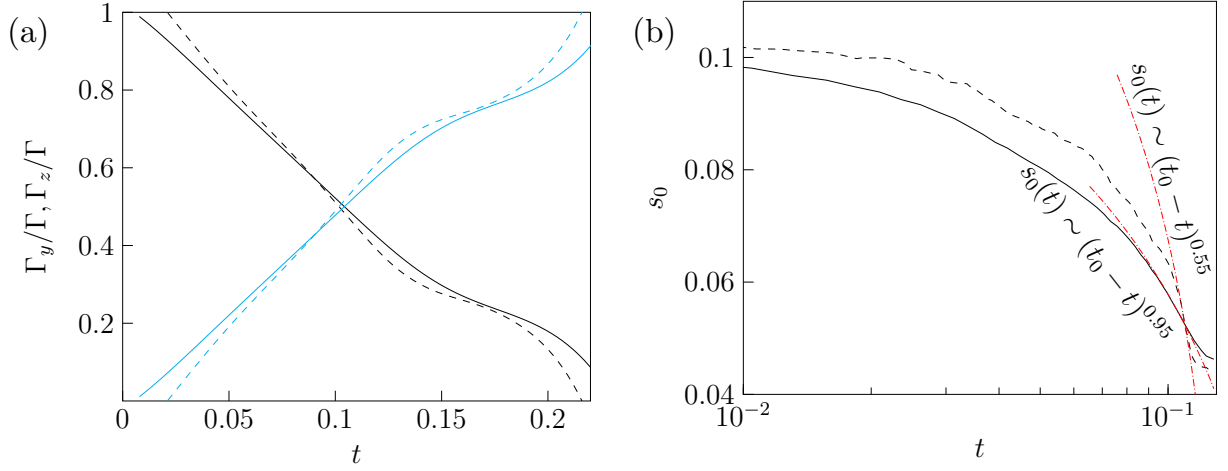


Figure 4: Temporal evolution of (a) circulation Γ_y, Γ_z normalized by the total circulation $\Gamma = \Gamma_y + \Gamma_z$ along the symmetric (x, z) plane shaded black and collision (x, y) plane shaded cyan respectively and (b) the separation distance s_0 is shown for both the Kida (solid line) and MK-type ring (dashed line) at $Re_\Gamma = 10^4$.

3 Results and discussion

Figure 2(a-e) shows the temporal evolution of vortex reconnection within the smaller box indicated in figure 1b for the Kida-type ring at $Re_\Gamma = 10^4$. The Q-criterion fields are thresholded at 10% of the maximum at each time step and shaded with axial vorticity ω_y to delineate the opposite rotation of the vortices. In the top panel, the first phase of reconnection, namely inviscid advection is evident. The anti-parallel vortex structures approach each other due to curvature-driven self-induction and collide. As explained in Kida et al. [1991], when the outermost vortex lines come into contact, they cancel each other at the point of contact due to viscous cross-diffusion. The process continues for other vortex lines forming hairpin-like bridge structures (see figure 1e) in a direction orthogonal to the initial approach of the two vortices. Since the hairpin-bridge structures are strongly curved at the tip, it generates a large self-induced velocity which pushes the structures outwards of the plane of the paper and backwards away from each other. This retreat also stops the cancellation of vortex lines and the remnant thread structures remain connected. Only the tail portion of the thread structure is visible as shown in figure 1f.

The entire process including core compression is better illustrated in figure 3(a-d) where contours of axial vorticity along the symmetric plane (x, z) are plotted at various times. The core becomes flatter upon approach, resulting in a head-tail dipole structure. Extending the results of YH and contradicting MK, the vortex core flattens further and almost smears out with increasing Re_Γ , even when the core is thin, as evidenced in figure 3(e-h) where contours of axial vorticity are plotted for the MK-type ring at $t = 0.115$.

A key evidence of reconnection is the transfer of circulation from the symmetry (x, z) plane to the collision plane (x, y) plane. This is calculated for one half of each plane with $\Gamma_y = \int \boldsymbol{\omega} \cdot \mathbf{n}_s dS$ and $\Gamma_z = \int \boldsymbol{\omega} \cdot \mathbf{n}_c dS$, where \mathbf{n}_s and \mathbf{n}_c are unit vectors normal to the symmetric and collision planes, and plotted in figure 4(a) for both Kida and MK-type rings at $Re_\Gamma = 10^4$. The inviscid advection phase is not evident as in YH due to the choice of the box (cf. figure 1(b)) where the complete vortex core is not visible during the initial time (see figure 2(a)). Therefore, the circulation along the symmetry plane

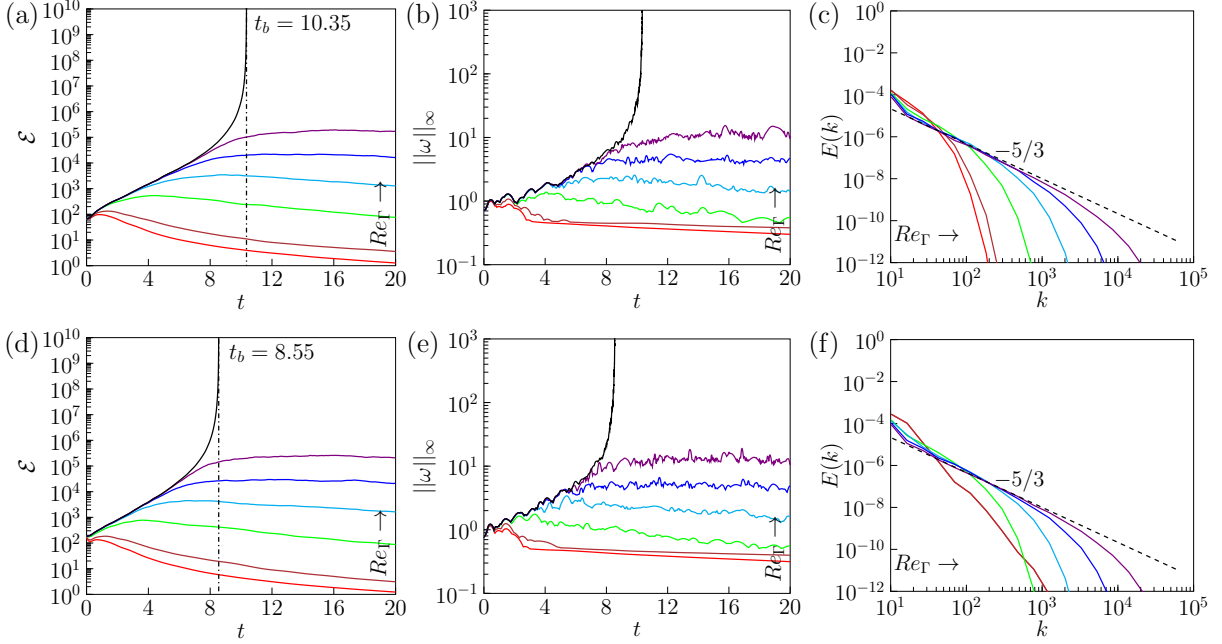


Figure 5: Time evolution of (a, d) total enstrophy \mathcal{E} , (b, e) maximum norm of vorticity $\|\omega\|_\infty$ and (c, f) kinetic energy spectrum at peak enstrophy for increasing Reynolds numbers. The top and bottom panels correspond to the Kida and MK-type rings respectively. $Re_\Gamma = \{5.10^3, 10^4, 10^5, 10^6, 10^7, 10^8, \infty\}$ are shaded red, maroon, green, cyan, blue, violet and black respectively.

initially increases as a larger portion of the vortex core comes into view. Later, a similar pattern as in YH is visible where the circulation continuously drops along the symmetry plane while consequently increasing along the collision plane.

An important question in reconnection studies is the rate of approach and separation of the vortices. If Γ is the only relevant dimensional quantity, it was shown with dimensional analysis that the separation distance s_0 would scale as $s_0 \sim (\Gamma t)^{1/2}$. Indeed, for quantized vortex reconnections with the Gross-Pitaevskii model, the approach and separation rates were found to follow the same scaling suggesting that this scaling may be universal [Villois et al., 2017]. However, Yao and Hussain [2020a] note that for viscous vortex reconnection, this scaling depends on the core size with slender cores maintaining the local assumption required for the $1/2$ scaling. To examine the temporal evolution of separation distance during approach, an approach similar to YH is taken where the centroid of ω_y at $0.75\omega_{y,\max}$ is calculated for one half of the symmetry plane and is taken to be the center of the tube. As shown in figure 4(b), the separation distance before reconnection is found to scale $s_0 \sim (t_0 - t)^{0.95}$ for the Kida-type ring, far from the $1/2$ scaling obtained from dimensional analysis. However, as found in Yao and Hussain [2020a], reducing the core size better maintains the local assumption and for the MK-type ring, s_0 scales as $(t_0 - t)^{0.55}$.

The temporal evolution of enstrophy and maximum norm of vorticity are plotted in figure 5(a, b) and figure 5(d, e) for the Kida and MK-type rings respectively. As explained in subsection 2.3, these quantities are calculated directly from lattice variables in Fourier space. This means that they are free from artefacts allowing us to examine for long times. It is clear that both enstrophy and vorticity, while increasing with Re_Γ , remain finite even for very large Re_Γ . Only the Euler simulation (indicated with a solid black line) shows a blowup for both cases, albeit at different times. This difference is

Re_Γ	Vortex ring thickness					
	$\delta_0/R = 0.2$			$\delta_0/R = 0.01$		
	Initial grid size	Final grid size	CPU time (s)	Initial grid size	Final grid size	CPU time (s)
10^4	$20 \times 40 \times 40$	$20 \times 40 \times 40$	11.15	$20 \times 40 \times 40$	$21 \times 42 \times 42$	18.27
10^8	$20 \times 40 \times 40$	$29 \times 58 \times 58$	45.44	$20 \times 40 \times 40$	$29 \times 58 \times 58$	21.31
∞	$20 \times 40 \times 40$	$64 \times 128 \times 128$	512.769	$20 \times 40 \times 40$	$65 \times 130 \times 130$	428.87
10^4	$21 \times 41 \times 41$	$21 \times 41 \times 41$	11.23	$21 \times 41 \times 41$	$22 \times 43 \times 43$	17.42
10^8	$21 \times 41 \times 41$	$40 \times 79 \times 79$	427.04	$21 \times 41 \times 41$	$41 \times 81 \times 81$	351.8
∞	$21 \times 41 \times 41$	$68 \times 135 \times 135$	1119.23	$21 \times 41 \times 41$	$79 \times 157 \times 157$	485.72

Table 1: Initial, final grid sizes and time taken for some cases of the log-lattice simulation. Bold font indicates simulations performed with the \mathbf{k}_0 mode. CPU time indicates the time taken for the convolution operation (3) at the last time step of the simulation.

to be expected as it is already shown by Pikeroen et al. [2024] that the blow-up time is sensitive to initial conditions. Figures 5(c, f) show the energy spectrum at peak enstrophy where one can observe a Kolmogorov-type $k^{-5/3}$ spectrum. At low Re_Γ , the range of the $-5/3$ slope is confined to the small wave numbers but this expands with increasing Re_Γ suggesting a large number of small-scale structures being generated as a result of successive reconnections.

4 Conclusion

With the log-lattice technique, numerical simulations of two inclined vortex rings with core sizes $\delta_0/R = 0.2, 0.01$ are performed for increasing Re_Γ up to 10^8 , along with an inviscid (Euler) simulation. It is capable of preserving key physical processes seen in DNS including core flattening and the formation of hairpin-like bridge structures that suppress vorticity amplification. In line with the results of YH, the peak of the maximum norm of vorticity increases with Re_Γ but remains finite even at $Re_\Gamma = 10^8$ and a blowup is seen only for the inviscid case. Other qualitative results observed with DNS studies such as circulation transfer and separation distance scaling are also captured quite well by log-lattices making it a suitable simplified model to study vortex reconnections and its links to FTS at a much lower computational cost than DNS as shown in table 1.

While it is possible to use the inverse DFT to visualize the reconnection process, this is limited to early times due to the presence of artefacts that are a result of using non-uniform, non-integer Fourier modes. Further improvements can be focused on interpolating the Fourier modes to linearly-spaced integer values to not only suppress artefacts but also to employ the standard Fast Fourier Transform algorithms. The delta function can also be used to study other initial conditions such as vortex tubes by replacing the equation of a circle with that of a line and convolving with a 3D Gaussian to give it some thickness. This is at the core of our current efforts to study the interaction of vortex tubes with increasing complexity - by varying the circulation strength, core sizes and introducing axial flow in the vortex cores at very high Re_Γ . Such studies of asymmetrical reconnection could be useful in devising a method for directly identifying vortex reconnection in turbulent flow data which is a major challenge.

Acknowledgements

We thank Giorgio Krstulovic for suggesting the Dirac delta function to represent vortex rings in Fourier space.

Funding

This research has been funded through the Agence Nationale pour la Recherche, via the grants ANR TILT grant agreement no. ANR-20-CE30-0035 and ANR BANG grant agreement no. ANR-22-CE30-0025.

Data and code availability statement

The driver scripts and data generated from log-lattice simulations can be requested directly from the authors. The log-lattice python code used in the manuscript was developed by Amaury Barral as a part of his PhD work and is freely available along with a detailed documentation. See Barral et al. [2024] for more details.

References

- Jie Yao and Fazle Hussain. A physical model of turbulence cascade via vortex reconnection sequence and avalanche. *Journal of Fluid Mechanics*, 883:A51, 2020a.
- Jie Yao and Fazle Hussain. Vortex reconnection and turbulence cascade. *Annual Review of Fluid Mechanics*, 54(1):317–347, 2022.
- Yoshifumi Kimura and HK Moffatt. Scaling properties towards vortex reconnection under biot–savart evolution. *Fluid Dynamics Research*, 50(1):011409, 2017.
- HK Moffatt and Yoshifumi Kimura. Towards a finite-time singularity of the navier–stokes equations. part 2. vortex reconnection and singularity evasion. *Journal of Fluid Mechanics*, 870:R1, 2019a.
- HK Moffatt and Yoshifumi Kimura. Towards a finite-time singularity of the navier–stokes equations. part 2. vortex reconnection and singularity evasion. *Journal of Fluid Mechanics*, 870:R1, 2019b.
- J Thomas Beale, Tosio Kato, and Andrew Majda. Remarks on the breakdown of smooth solutions for the 3-d euler equations. *Communications in Mathematical Physics*, 94(1):61–66, 1984.
- Jie Yao and Fazle Hussain. On singularity formation via viscous vortex reconnection. *Journal of Fluid Mechanics*, 888:R2, 2020b.
- S Kida, M Takaoka, and Fazle Hussain. Collision of two vortex rings. *Journal of Fluid Mechanics*, 230:583–646, 1991.
- Ciro S Campolina and Alexei A Mailybaev. Fluid dynamics on logarithmic lattices. *Nonlinearity*, 34(7):4684, 2021.

- Luca Biferale. Shell models of energy cascade in turbulence. *Annual review of fluid mechanics*, 35(1):441–468, 2003.
- Ciro S Campolina and Alexei A Mailybaev. Chaotic blowup in the 3d incompressible euler equations on a logarithmic lattice. *Physical review letters*, 121(6):064501, 2018.
- Tomas Bohr, Mogens H Jensen, Giovanni Paladin, and Angelo Vulpiani. *Dynamical systems approach to turbulence*. 1998.
- Özgür D Gürçan. Nested polyhedra model of turbulence. *Physical Review E*, 95(6):063102, 2017.
- Amaury Barral and Berengere Dubrulle. Asymptotic ultimate regime of homogeneous rayleigh–bénard convection on logarithmic lattices. *Journal of Fluid Mechanics*, 962:A2, 2023.
- Julian CR Hunt, Alan A Wray, and Parviz Moin. Eddies, streams, and convergence zones in turbulent flows. *Studying turbulence using numerical simulation databases, 2. Proceedings of the 1988 summer program*, 1988.
- Hans J Lugt. The dilemma of defining a vortex. In *Recent developments in theoretical and experimental fluid mechanics: Compressible and incompressible flows*, pages 309–321. Springer, 1979.
- Pinaki Chakraborty, Sivaramakrishnan Balachandar, and Ronald J Adrian. On the relationships between local vortex identification schemes. *Journal of fluid mechanics*, 535:189–214, 2005.
- Alberto Villois, Davide Proment, and Giorgio Krstulovic. Universal and nonuniversal aspects of vortex reconnections in superfluids. *Physical Review Fluids*, 2(4):044701, 2017.
- Quentin Pikeroen, Amaury Barral, Guillaume Costa, Ciro Campolina, Alexei Mailybaev, and Berengere Dubrulle. Tracking complex singularities of fluids on log-lattices. *Non-linearity*, 37(11):115003, 2024.
- Amaury Barral, Bérengère Dubrulle, Guillaume Costa, Quentin Pikeroen, and Adrien Lopez. Pyloggrid: A python package for fluid dynamics on logarithmic lattices. *Journal of Open Source Software*, 9(104):6439, 2024.